Check for updates

Experimental and computational study of the exchange interaction between the V(III) centers in the vanadium-cyclal dimer†

Andreas Reiß,[a] Maximilian Kai Reimann, [ID] [b] Chengyu Jin,[c] Martha Wachter-Lehn,[d] Reinhard K. Kremer, [ID] [e] Rainer Pöttgen, [ID] [b] Karin Fink, [ID] [c] Wim Klopper [ID] *[c,d] and Claus Feldmann [ID] *[a]

[V_2(HCyclal)$_2$] is prepared by controlled oxidation of vanadium nanoparticles at 50 °C in toluene. The V(0) nanoparticles are synthesized in THF by reduction of VCl_3 with lithium naphthalenide. They exhibit very small particle sizes of 1.2 ± 0.2 nm and a high reactivity (*e.g.* with air or water). By reaction of V(0) nanoparticles with the azacrown ether H_4Cyclal, [V_2(HCyclal)$_2$] is obtained with deep green crystals and high yield. The title compound exhibits a V(III) dimer (V···V: 304.1(1) pm) with two deprotonated [HCyclal]$^{3-}$ ligands as anions. V(0) nanoparticles as well as the sole coordination of V(III) by a crown ether as the ligand and nitrogen as sole coordinating atom are shown for the first time. Magnetic measurements and computational results point to antiferromagnetic coupling within the V(III) couple, establishing an antiferromagnetic spin $S = 1$ dimer with the magnetic susceptibility determined by the thermal population of the total spin ranging from $S^T = 0$ to $S^T = 2$.

Introduction

Binuclear coordination compounds with M···M dimers (M: metal) and certain binding between the metal atoms are well-known and have been intensely studied.[1] Prominent examples comprise Mg–Mg, Re≡Re, W≡W, or Cr≡Cr dimers with the respective single to fourfold bonding.[2] Typical methods to prove the type of metal–metal interaction are crystal-structure analysis (*e.g.* evaluation of M···M distance), magnetism (*e.g.* presence/absence of non-paired electrons), or computational results (*e.g.* analysis of bonding situation).[1,2] In the case of vanadium, a wide variety of binuclear compounds ranging from V(I),[3] V(II)[4] *via* V(III)[5] to V(IV)[6] with different interaction of

the vanadium dimer was reported. Most often chalcogenide-based ligands were used to coordinate and to stabilize the V_2 dimer. As a synthesis approach, the reduction of vanadium species with a higher oxidation state (most often V(IV), V(V)) is the most widely applied.[3–6]

As a part of our studies on the synthesis of base-metal nanoparticles and their reactivity,[7] we have realized zerovalent vanadium (V(0)) nanoparticles, which we present here for the first time. The synthesis of V(0) nanoparticles follows our general approach of reducing metal halides after dissolution in tetrahydrofuran (THF) with a solution of lithium or sodium naphthalenide ([LiNaph], [NaNaph]) in THF. This liquid-phase synthesis typically results in 1–5 nm-sized metal nanoparticles and is suitable for a large group of base-metal nanoparticles (*i.e.* Mg, Al, all group IIIb to group VIIb transition metals, all rare-earth metals from Sc to Lu).[7,8] At present, the knowledge on V(0) nanoparticles is low and limited to gas-phase methods.[9] Moreover, a stabilization of the metal core against oxidation by a vanadium carbide shell as passivating layer was described.[10] However, a reliable synthesis strategy for V(0) nanoparticles <10 nm is unknown, so far. This situation can be also related to the absence of chemically stable vanadium carbonyls as starting materials, which, therefore, cannot be thermally decomposed in the liquid phase as in the case of other transition metals (*e.g.*, Cr, Mn, Fe, Co).[11]

With this study, we present a reliable liquid-phase synthesis of V(0) nanoparticles with a size <10 nm. To evaluate their

[a]Institut für Anorganische Chemie, Karlsruhe Institute of Technology (KIT), Engesserstraße 15, 76131 Karlsruhe, Germany. E-mail: claus.feldmann@kit.edu
[b]Institut für Anorganische und Analytische Chemie, Universität Münster, Corrensstraße 30, 48149 Münster, Germany
[c]Institut für Nanotechnologie, Karlsruhe Institute of Technology (KIT), Hermann-von-Helmholtz-Platz 1, 76344 Eggenstein-Leopoldshafen, Germany
[d]Institut für Physikalische Chemie, Karlsruhe Institute of Technology (KIT), Fritz-Haber-Weg 2, 76131 Karlsruhe, Germany
[e]Max-Planck-Institut für Festkörperforschung, Heisenbergstraße 1, 70569 Stuttgart, Germany

reactivity in the liquid phase near room temperature (≤100 °C),[12] we exemplarily show the reaction and reactivity of the V(0) nanoparticles with an azacrown ether to obtain single crystals of [V$_2$(HCyclal)$_2$]. [V$_2$(HCyclal)$_2$] contains a dimer of V(III) cations, which show antiferromagnetic coupling and a rare coordination of vanadium, only with the azacrown ether as a ligand and nitrogen as sole donor atom. The exchange interaction between the V(III) centers is analysed based on magnetic measurements and computational studies.

Experimental section

General

All sample handling and reactions were performed under argon atmosphere using standard Schlenk techniques and gloveboxes (MBraun Unilab, O$_2$/H$_2$O < 0.1 ppm). Reactions were carried out in Schlenk flasks or glass ampoules. Prior to use, all glassware was evacuated ($p \leq 10^{-3}$ mbar), heated, and flushed with argon thrice to remove all moisture.

Chemicals

Tetrahydrofurane (THF, Seulberger, 99%) and toluene (Seulberger, 99%) were refluxed over sodium with benzophenone and distilled off prior to use. Lithium metal (Alfa Aesar, 99%) was freshly cut under argon atmosphere prior to use. 1,4,8,12-Tetraazacyclopentadecane (H$_4$Cyclal, Sigma-Aldrich, 97%), naphthalene (Alfa Aesar, ≥99%), and VCl$_3$ (Alfa Aesar, 99%) were used as purchased.

V(0) nanoparticles

16.7 mg of lithium (2.40 mmol), 323.0 mg of naphthalene (2.52 mmol), and 125.8 mg of VCl$_3$ (0.80 mmol) were dissolved in 15 mL of THF and stirred for 12 hours, resulting in a deep black suspension. The as-prepared V(0) nanoparticles were separated by centrifugation (45 000g) and purified by washing twice with 15 mL of THF. Finally, the V(0) nanoparticles were redispersed in THF to obtain long-term stable suspensions or dried in vacuum to obtain powder samples with a yield of about 70%.

V$_2$(HCyclal)$_2$ (1)

25.7 mg of dried V(0) nanoparticles (0.51 mmol), 108.4 mg of H$_4$Cyclal (0.51 mmol), and 0.4 mL of toluene were filled into a Schlenk tube. The Schlenk tube was heated to 50 °C for 7 days. After natural cooling to room temperature, deep green crystals of **1** were obtained with a yield of about 75% in relation to the employed amount of H$_4$Cyclal. The title compound is sensitive to air and moisture and readily oxidized, generating a brown, amorphous crust covering the crystal surfaces of **1**.

Analytical equipment

Details related to analytical techniques, crystallographic data, and computational methods are described in the ESI.†

Results and discussion

Synthesis and characterization of V(0) nanoparticles

Zerovalent vanadium nanoparticles were prepared utilizing a general synthesis strategy to realize zerovalent base-metal nanoparticles *via* naphthalenide-driven reduction of simple metal halides, which we established recently.[7,8] To obtain zerovalent vanadium (V(0)) nanoparticles, VCl$_3$ was used as the starting material, lithium naphthalenide ([LiNaph]) as the reducing agent, and tetrahydrofuran (THF) as the solvent (Fig. 1). Due to the low solubility of VCl$_3$ in THF, VCl$_3$, lithium metal and naphthalene were added to THF in a one-pot approach (Fig. 1a). Thus, VCl$_3$ largely remains as an insoluble solid at the bottom of the Schlenk tube, and lithium metal is located on top of the liquid phase due to its low density. Upon intense stirring over 12 hours, [LiNaph] is formed resulting in a greenish solution. VCl$_3$ is slowly dissolved, but – after dissolution – instantaneously reacts with [LiNaph] to form V(0) nanoparticles. Despite these – from a general perspective – non-optimal conditions for nanoparticle nucleation (*i.e.*, lithium and VCl$_3$ as solid phases instead of a homogeneous solution), two essential aspects nevertheless promote the nucleation of very small nanoparticles. First, the reduction of VCl$_3$ is very fast. Second, the solubility of zerovalent vanadium in THF is extremely low, so that a high supersaturation is
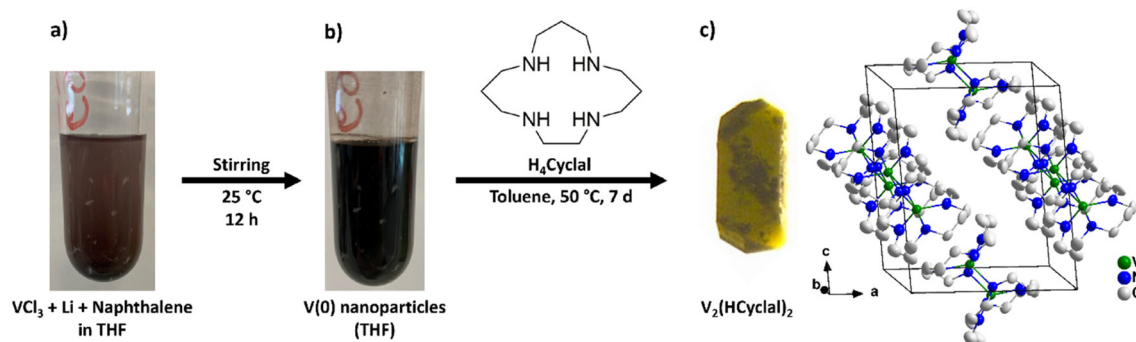

Fig. 1 Scheme illustrating the synthesis of V(0) nanoparticles with (a) starting materials, (b) the as-prepared V(0) nanoparticles in THF, (c) single crystal and unit cell of [V$_2$(HCyclal)$_2$] after liquid-phase oxidation of the V(0) nanoparticles.

reached. In sum, VCl_3 and lithium metal have reacted completely after 12 hours of vigorous stirring, resulting in a deep black suspension of V(0) nanoparticles (Fig. 1b).

The V(0) nanoparticles were purified by centrifugation and repeated redispersion/centrifugation in/from THF to remove LiCl and naphthalene. Thereafter, the nanoparticles can be redispersed either in THF or in toluene to obtain colloidally stable suspensions, or they can be dried in vacuum to obtain powder samples. For their handling, caution needs to be paid since the V(0) nanoparticle suspensions and powder samples are highly reactive when in contact to O_2, H_2O or other oxidizing agents. Specifically, the reaction of powder samples with oxygen and/or water can result in violent reactions and explosions. Consequently, the V(0) nanoparticles need to be handled and stored under inert conditions (argon, nitrogen).

Particle size and shape of the V(0) nanoparticles were examined by transmission electron microscopy (TEM). Accordingly, spherical nanoparticles with uniform size were obtained with a size range of 1–2 nm and a low degree of agglomeration (Fig. 2a). Statistical evaluation of >200 nanoparticles on TEM images results in a mean diameter of 1.2 ± 0.2 nm (Fig. 2c). High-resolution (HR)TEM images prove the as-prepared V(0) nanoparticles to be monocrystalline with lattice fringes through the whole particle (Fig. 2b). The lattice plane distance of 2.1 ± 0.1 Å is in good agreement with cubic bulk vanadium (V(0): d_{110} with 2.1 Å).[13] Composition and surface functionalization of the as-prepared V(0) nanoparticles were further exam-

ined by Fourier-transform infrared (FT-IR) spectroscopy and element analysis (EA). FT-IR spectra, as expected, indicate the solvent THF to be adsorbed on the particle surface (Fig. 2d). The observed weak vibrations relate to THF (ν(C–H): 3000–2800 cm^{-1}, ν(C–O): 1100–900 cm^{-1}, fingerprint area: 1500–500 cm^{-1}). EA indicates C and H contents of 53.4 and 4.1 wt% with a C : H ratio of 13, which is higher as expected for THF (C : H = 6). This indicates certain amount of naphthalene also to be adhered on the particle surface. The comparably high C/H content is to be expected in view of the small particle size (1.2 ± 0.2 nm) and a monomolecular adsorption layer. Finally, it must be noticed that the synthesis of V(0) nanoparticles with [LiNaph] is the first liquid-phase synthesis of vanadium nanoparticles with a diameter <10 nm until now.

Synthesis and structure of [V₂(HCyclal)₂]

The reaction of, for instance, oxygen or water already points to the high reactivity of the as-prepared V(0) nanoparticles. As expected, the reactivity of the V(0) nanoparticles is much higher as compared to bulk vanadium. This high reactivity already indicates the absence of passivation layers (e.g. vanadium oxides/hydroxides). Violent reactions such as in air or in water, however, are not controlled in terms of reproducible conditions or the formation of a specific compound. To probe the reactivity of the V(0) nanoparticles and to perform a reaction in a controlled manner, we have reacted them in the liquid phase near room temperature (≤100 °C) with the aza-
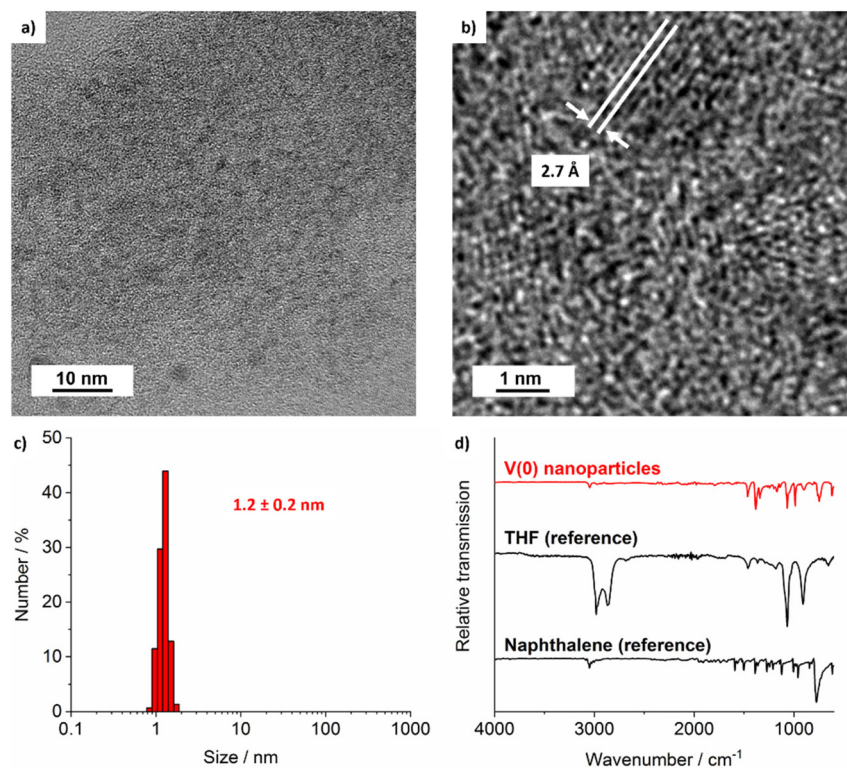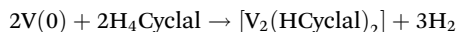

Fig. 2 Characterization of the as-prepared V(0) nanoparticles: (a) TEM overview image, (b) single V(0) nanoparticle with lattice fringes, (c) size distribution (based on statistical evaluation of >200 nanoparticles on TEM images), (d) FT-IR spectrum (with THF and naphthalene as references).

crown ether 1,4,8,12-tetraazacyclopentadecane (H$_4$Cyclal) as a mild oxidizing agent and sterically demanding ligand. This seemed specifically promising in regard of the different oxidation states of vanadium between ±0 and +V as well as in regard of a potential metal–metal interaction. For this purpose, the V(0) nanoparticles were reacted with H$_4$Cyclal at 50 °C in toluene for 7 days, which results in the formation of deep green, moisture- and air-sensitive single crystals of V$_2$(HCyclal)$_2$ with visible evolution of hydrogen (Fig. 1c). The title compound was obtained with a yield of about 75% (in relation the applied amount of V(0) nanoparticles). The synthesis can be ascribed to the following reaction:

$$2V(0) + 2H_4Cyclal \rightarrow [V_2(HCyclal)_2] + 3H_2$$

According to single-crystal structure analysis, [V$_2$(HCyclal)$_2$] crystallizes in the monoclinic space group $P2_1/n$ (ESI: Table S1 and Fig. S1†). The title compound is composed of a binuclear vanadium-cyclal complex, in which each V center is trigonal-bipyramidally coordinated by four nitrogen atoms of one azacrown ether and one nitrogen atom of the second azacrown ether (Fig. 3; ESI: Fig. S2†). Furthermore, one nitrogen atom of both azacrown ethers shows μ$_2$-bridging of the V$_2$ couple. Here, it needs to be noticed that the azacrown ether is disordered in the crystal structure, so that the propyl and ethyl groups of the azacrown ether cannot be localized in a specific position. In the structure refinement, this was taken care of by assuming split-atom positions with 50% occupancy for each atom (ESI: Fig. S3†). The V–N distances amount to 209.9(9) pm (N1′) and 215.0(10) pm (N1) within the V$_2$N$_2$ ring as well as to 191.8(7) (N2), 200.9(13) (N3), and 224.3(5) (N4) to the non-bridging N atoms. The comparably high standard deviations observed for the V–N distances can be attributed to the aforementioned disorder of the azacrown-ether ligands. The angles in the V$_2$N$_2$ quadrangle (N1–V1–N1′: 88.6(4), V1–N1–V1′: 91.4(4)°) are in accordance with the different distances and the deviation from an ideal squared arrangement. As expected, the

bridging N atoms (N1, N1′) show larger V–N distances than N2 and N3. The longest V–N distance, however, is observed for N4 and – together with the V–N–C angles of 109.4(6)–116.0(6)° – indicates a tetrahedral arrangement with a non-protonated NH group. In contrast, N1 to N3 are deprotonated as indicated by V–N–C angles of 115.3(5)–134.2(7)°, corresponding to a distorted trigonal planar coordination. In sum, this points to the presence of an (HCyclal)$^{3-}$ ligand and, *vice versa*, an oxidation state of +III of vanadium. This oxidation state is also in accordance with the deep green color of the title compound (Fig. 1c) and further validated by magnetic measurements and computational analysis (see below). A coordination of vanadium by crown ethers as a ligand is rare, even with the most conventional crown ethers 15-crown-5 or 18-crown-6.[14] Most often thiol crown ethers were used as ligands.[15] A coordination with azacrown ethers was only reported for [V(IV)O(cyclam)Cl]Cl[16] and [(cyclen)V(III)(CN)$_3$],[17] which both represent mononuclear coordination compounds with additional ligands coordinated to the vanadium center. Moreover, [V(IV)O(cyclam)Cl]Cl and [(cyclen)V(III)(CN)$_3$] were prepared *via* Lewis-acid–base reactions with VO(SO$_4$) or VCl$_3$ as starting materials, and the azacrown ether serves as neutral ligand without any deprotonation.[16,17]

Beside single-crystal structure analysis, structure and purity of the title compound were validated by X-ray powder diffraction (ESI: Fig. S4†). To verify the presence of a remaining NH group of the azacrown ether, Fourier-transform infrared (FT-IR) spectroscopy was performed and compared to the pure ligand H$_4$Cyclal (Fig. 4). In general, all vibrations of the ligand are visible for the title compound. Intensity, splitting, and position of the vibrations are of course slightly different to the free, non-bound ligand due to the different point symmetry and binding situation. In regard of the N–H vibrations at 3300–3000 cm^{-1}, the intensity is significantly lower for [V$_2$(HCyclal)$_2$] as for free H$_4$Cyclal. However, the N–H vibrations are still visible, which is in accordance with a partial deprotonation of the azacrown ether (Fig. 4). Together with the tetrahedral arrangement of a sole nitrogen atom, FT-IR spectra confirms the presence of a remaining NH-group of the (HCyclal)$^{3-}$ anion.
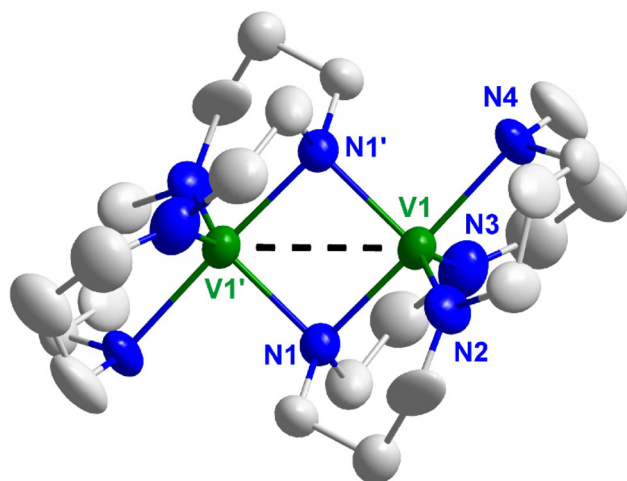

Fig. 3 Molecular structure of [V$_2$(HCyclal)$_2$] (disorder of azacrown ether and H atoms not shown for clarity).
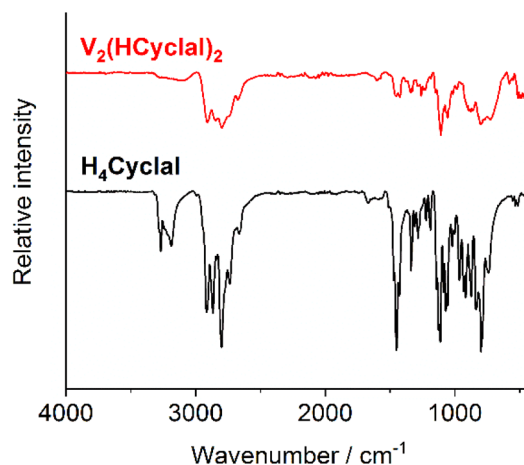

Fig. 4 FT-IR spectra of V$_2$(HCyclal)$_2$ and H$_4$Cyclal as a reference.

Table 1 V–V distance of [V$_2$(HCyclal)$_2$] in comparison to literature-known compounds

Compound	V–V distance/pm	Oxidation state of V
K(THF)$_3$[V^{+I}V^{+II}(DPhF)$_4$]^3	192.95(8)	+I/+II
[V$^{+II}_2$(hpp)$_4$]^{4a}	193.2(1)	+II
[V$^{+II}_2$(DFM)$_4$]^{4b}	197.5(4)	
[V$^{+II}_2$(2,6-dimethoxyphenyl)$_4$]^{4c}	220.0(2)	
[V$^{+III}_2$(salophen)$_2$Na$_2$(THF)$_6$]^{5a}	240.6(3)	+III
[V$^{+III}_6$Se$_8$O(PMe$_3$)$_6$]^{5b}	279.4–283.9	
[(π-MeC$_5$H$_4$)$_4$V$^{+III}_4$(μ$_3$-S)$_4$]^{5c}	286.5–287.0	
[V$^{+III}_2$(HCyclal)$_2$] (title compound)	304.1(1)	
[(π-MeC$_5$H$_4$)$_5$V$^{+III}_4$V^{+IV}(μ$_3$-S)$_6$]^{5d}	305.9(2)–321.7(2)	+III/+IV
[V$^{+IV}_2$(μ-S$_2$)$_2${(C$_4$H$_9$)$_2$NCS$_2$}$_4$]^{6a}	285.1	+IV
[V$^{+IV}_2$(S$_2$)$_2$(S$_2$CNEt$_2$)$_4$]^{6b}	288.4	

DPhF: *N,N′*-diphenylformamidine; hpp: 1,3,4,6,7,8-hexahydro-2*H*-pyrimido[1,2-*a*]pyrimidin; DFM: *N,N′*-di-(*p*-tolyl)formamidinate.

The V–V distance in [V$_2$(HCyclal)$_2$] is 304.1(1) pm, which indicates an interaction of the V(III) dimer. In comparison to other dinuclear vanadium units, however, this distance is at the upper end of observed separation (Table 1). Most often dimers of V(II) were reported that exhibit a significantly shorter threefold V≡V bond. V(III) dimers, typically with chalcogenide-type ligands, also exhibit distances below about 290 pm (Table 1). In this regard, it needs to be noticed that [V$_2$(HCyclal)$_2$] is the only V(III) dimer with sole coordination by nitrogen.

Magnetic properties of [V$_2$(HCyclal)$_2$]

To verify the interaction within the V$_2$ dimer in [V$_2$(HCyclal)$_2$], magnetic measurements were performed with the molar susceptibility determined in an external magnetic field of 10 kOe (Fig. 5a). Apart from a strong divergence of the susceptibility towards lowest temperatures, which can be ascribed to Curie-like susceptibility contributions from free V(III) entities, the increase of the magnetic susceptibility with increasing temperature is characteristic and indicates a gradual thermal population of excited states with a magnetic moment.

To describe the susceptibility of the title compound, each V(III) cation is assumed to have a $S = 1$ state, *i.e.*, an orbital singlet of
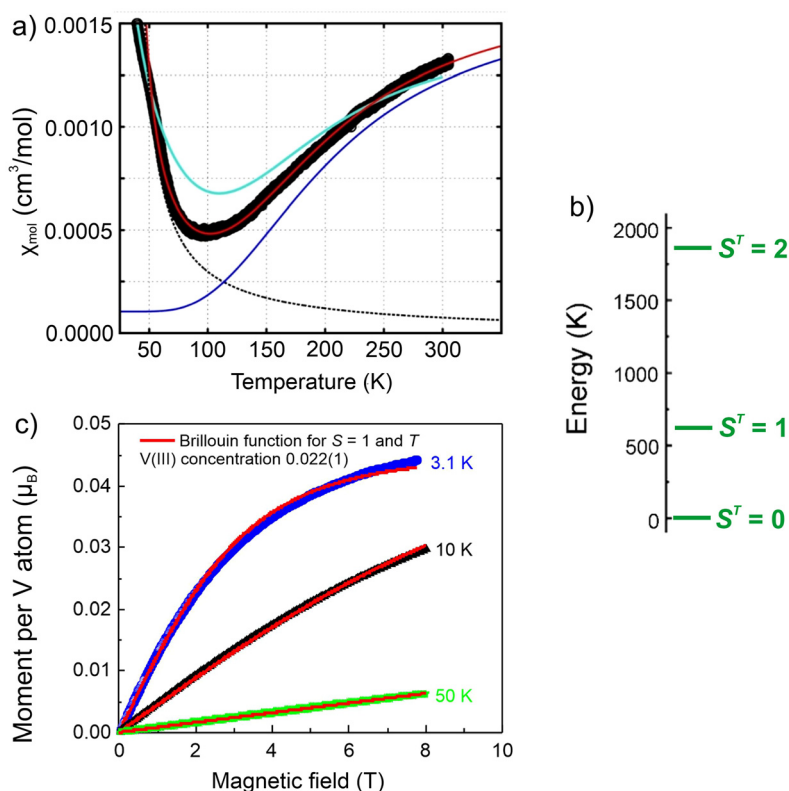

Fig. 5 Temperature-dependent molar susceptibility of [V$_2$(HCyclal)$_2$]: (a) experimental molar susceptibility per two V(III) centers (filled black circles) and calculation (red solid line, based on eqn (1) (solid blue line) to which a Curie–Weiss term (black dashed line) of the form $c/(T - T_c)$ was added (c = 0.02 cm^3 mol^{-1} K, T_c = 33 K) with antiferromagnetic spin exchange of J = −299 K, a g-factor of 2.06, and a temperature-independent contribution (TIC) of χ_0 = 1.04 × 10^{-4} cm^3 mol^{-1}. The turquoise solid line shows the result from fitting only J = −289 K with the program PHI, without TIC but with a paramagnetic triplet impurity of 6%; (b) energy diagram for a $S = 1$ dinuclear unit with an antiferromagnetic spin exchange of J = −299 K. (c) Magnetization isotherms of [V$_2$(HCyclal)$_2$] recorded at 3.1, 10 and 50 K. The red lines correspond to fits according to an $S = 1$ Brillouin function. The refined concentration of free V(III) is indicated and consistent with the data in (a).

the ^{3}F d^2 ground state and an antiferromagnetic spin–spin coupling of the nearby V(III) cations, 302 pm in distance, to a dinuclear unit. The Hamiltonian of such dinuclear unit is given by:

$$\mathcal{H} = -2JS_1S_2$$

where S_1 and S_2 denote the spins of the two V(III) centers in the dinuclear unit and J the spin–spin exchange between them. In the case of antiferromagnetic coupling ($J < 0$), the spin exchange couples the two spins to a total spin singlet $S^T = 0$ (ground state), with $S^T = 1$ and $S^T = 2$ as excited states. These are located by $-2J$ and $-6J$ above the singlet ground state.

The magnetic susceptibility of such a spin $S = 1$ dinuclear unit (for two V(III) centers) is given by:[18]

$$\chi_{\mathrm{mol}}(T) = 2N_A \frac{\mu_0\mu_B{}^2 g^2}{3k_B T}\frac{D}{Z} + \chi_0 \tag{1a}$$

with

$$D = \{3\exp(2x) + 15\exp(6x)\} \tag{1b}$$

and

$$Z = \{1 + 3\exp(2x) + 5\exp(6x)\} \tag{1c}$$

and

$$x = \frac{J}{k_B T} \tag{1d}$$

χ_0 takes care of temperature-independent diamagnetic and van Vleck contributions. Here, we have neglected any zero-field splitting of the individual S_i spin states and any anisotropy of the g-factor. The calculation reproduces the growth of the susceptibility with increasing temperature quite well, using a g-factor of 2, the latter being close to what has been observed for isolated V(III) centers by electron paramagnetic resonance.[19] The energy level diagram of a $S = 1$ dinuclear unit, coupled by an antiferromagnetic spin exchange of -299 K is shown in Fig. 5b. The antiferromagnetic ground state is also in agreement with the magnetization isotherms. Thus, the magnetic moment per vanadium atom is only $0.05\mu_B$ at 3.1 K and 80 kOe. The magnetization isotherms recorded at 3.1, 10 and 50 K are shown along with Brillouin fits for $S = 1$ (Fig. 5c). At 300 K, $\chi T = 0.390$ cm^3 mol^{-1} K is rather small, which can be ascribed to the strong antiferromagnetic coupling.[20] Only 30% of the dimer molecules are in the $S^T = 1$ state, and the $S^T = 2$ state remains virtually unoccupied (ESI: Table S5 and Fig. S5†).

Computation of exchange interactions

The experimental findings are confirmed by *ab initio* quantum-chemical calculations, both by density-functional-theory (DFT) calculations and configuration-interaction (CI) calculations (see ESI† for details). The calculations reveal that the dinuclear V(III) complex [V$_2$(HCyclal)$_2$] can be described perfectly well in terms of two antiferromagnetically coupled 3d^2 centers with spins $S_1 = S_2 = 1$.

DFT calculations were performed at the B3LYP-D3(BJ)-abc level using the def2-TZVPP basis set for vanadium and nitro-
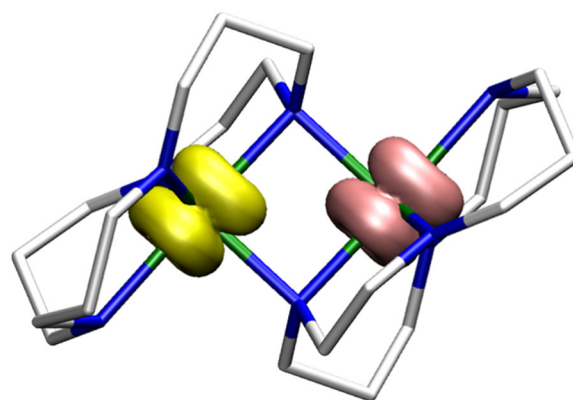

Fig. 6 Spin density (plotted at an isovalue of $\pm 0.02a_0{}^{-3}$) of the broken-symmetry Kohn–Sham determinant as obtained at the B3LYP-D3(BJ)-abc level (H atoms omitted for clarity).

gen, the def2-TZVP basis for carbon, and the def2-SV(P) basis for hydrogen (ESI: Table S2†). Since the open-shell singlet ground state of the complex cannot be described by a single Kohn–Sham determinant, we have approximated the energy of the ground state (GS) as a linear combination of the energies of the high-spin (HS) determinant (with $M_{S_1} = 1$ and $M_{S_2} = 1$; $\langle\hat{S}^2\rangle \approx 6\hbar^2$) and a broken-symmetry (BS, Fig. 6) determinant with $M_{S_1} = 1$, $M_{S_2} = -1$, and $\langle\hat{S}^2\rangle \approx 2\hbar^2$:

$$E_{\mathrm{GS}} = \frac{3}{2}E_{\mathrm{BS}} - \frac{1}{2}E_{\mathrm{HS}} \tag{2}$$

This equation follows from assuming that the relevant $\langle\hat{S}^2\rangle$ expectation values are equal to $6\hbar^2$ and $2\hbar^2$, thereby neglecting the dependence of the geometry on these expectation values.[21–23]

After optimizing the ground-state geometry, which displays C_i point-group symmetry, the exchange coupling parameter was computed according to the formula:

$$J = \frac{1}{6}(E_{\mathrm{GS}} - E_{\mathrm{HS}}) = \frac{1}{4}(E_{\mathrm{BS}} - E_{\mathrm{HS}}) \tag{3}$$

At the B3LYP-D3(BJ)-abc level, we obtained $J = -251$ K at the optimized ground-state geometry. We have repeated the DFT calculations using the TPSSh functional (ESI: Table S3†), but the geometry optimization with this functional yielded a much too short V–V distance (Table 2). Therefore, we decided to

Table 2 Structural parameters of [V$_2$(HCyclal)$_2$] from geometry optimizations at the B3LYP-D3(BJ)-abc and TPSSh-D3(BJ)-abc levels

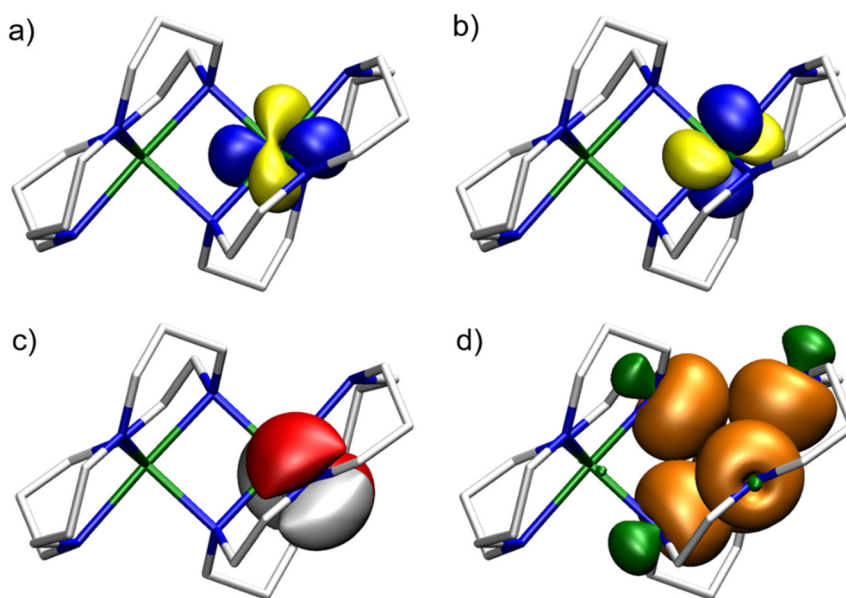| Parameter	TPSSh	B3LYP	Exptl.
V1–V1 distance (pm)	288.6	301.4	304.1(1)
V1–N1 distance (pm)	211.9	214.7	215.8(10)
V1–N1′ distance (pm)	207.1	208.6	209.9(9)
V1–N2 distance (pm)	194.9	195.1	191.8(7)
V1–N3 distance (pm)	192.6	193.3	200.9(13)
V1–N4 distance (pm)	225.2	227.1	224.3(5)
N1–V–N1′ angle (°)	92.9	89.2	88.6(4) and 89.0(4)
V1–N1–V1′ angle (°)	87.1	90.8	91.0(4) and 91.4(4)

Fig. 7 Localized spin orbitals that describe the bonding situation in the $[V_2(HCyclal)_2]$ complex, plotted at an isovalue of $\pm 0.05 a_0^{-3/2}$: (a) first singly occupied 3d orbital on V1. (b) Second singly occupied 3d orbital on V1. (c) Two 2p orbitals on N2 and N3 with π-donating character. (d) Five σ-donor orbitals (of which four are visible).

adopt the B3LYP optimized structure for our investigations at the CI level. Note that also the N1–V–N1′ and V1–N1–V1′ angles (being decisive for the strength of the exchange coupling) of the B3LYP geometry agree much better with those of the experimental X-ray structure than the TPSSh ones.

Finally, we show localized (majority-spin) spin–orbitals of the $[V_2(HCyclal)_2]$ complex as obtained for the high-spin state ($M_S = 2$). Fig. 7 shows the coordination of one of the two equivalent V(III) centers. The same orbitals are also found on the other V(III) center. Each V(III) center has two singly occupied 3d orbitals and is coordinated by five N atoms, which all contribute one σ-donor orbital. The atoms N1, N1′ and N4 are sp^3-hybridized and only contribute a single σ-donor orbital. The atoms N2 and N3, however, are sp^2-hybridized and their lone-pair 2p-orbital shows π-donating character towards to V(III) center, leading to V1–N2 and V1–N3 distances that are about 23–25 pm shorter than the other three V1–N bond distances.

Based on the B3LYP-D3(BJ)-abc optimized structure of the singlet state, modified complete-active-space configuration-interaction (modified CASCI) calculations[24] were performed in a (4,4) active space of the partly occupied 3d orbitals with the complete-active-space spin–orbit configuration interaction (CASOCI)[25] program (ESI: Table S4†). The charge-transfer states were shifted down by 11.48 eV. The calculated susceptibilities are compared to the measured data (ESI: Fig. S5†). This approach yielded a magnetic exchange coupling constant of $J = 247$ K. Assuming a paramagnetic impurity of 6% by a potential V(III) monomer in a triplet state, J was fitted with the program PHI[26] to the experimental data with $J = -289$ K as best value. Though the calculated and fitted values of the magnetic exchange constants show some differences in the exact value, all of them show a strong antiferromagnetic coupling of

the two vanadium centers with an overall singlet ground state. At temperatures below 50 K, the occupation of higher states is neglectable (ESI: Table S5†). The strong increase below 50 K must be connected to a paramagnetic impurity. Even at higher temperatures, the absolut value of the magnetic susceptibility remains rather small due to the strong coupling. At 300 K, 69% of the $[V_2(HCyclal)_2]$ molecules are in the singlet ground state, 30% in the triplet state, and 1% in the quintet state (ESI: Table S5†). This corresponds to $\chi T = 0.34$ cm^3 K mol^{-1}. Combining with 6% of a paramagnetic impurity and 94% of $V_2(HCyclal)_2$, $\chi T = 0.38$ cm^3 K mol^{-1}, is in good agreement with the experimental value.

Conclusion

$[V_2(HCyclal)_2]$ contains a novel V(III) dimer with the vanadium centers coordinated and bridged by deprotonated $[HCyclal]^{3-}$ azacrown ligands. Such coordination of vanadium only by crown ethers as ligands and with nitrogen as sole donor is reported here for the first time. The title compound was prepared by controlled oxidation of vanadium nanoparticles with the azacrown ether $H_4Cyclal$ in the liquid phase (toluene) near room temperature (50 °C). Such a redox approach was rarely reported and allows irreversible reactions due to the removal of hydrogen. Whereas bulk vanadium is more-or-less non-reactive at low temperature in the liquid phase, the as-used V(0) nanoparticles are highly suitable as starting material. They were synthesized in THF by reduction of VCl$_3$ with lithium naphthalenide and are characterised by a very small particle size of 1.2 ± 0.2 nm. Such V(0) nanoparticles and their use as a starting material open new options for reactions in the liquid

phase. The V(III) dimer (V⋯V: 304.1(1) pm) in $[V_2(HCyclal)_2]$ exhibits a very strong antiferromagnetic coupling of the two $S = 1$ centres to a spin-ladder ranging from $S^T = 0$ to $S^T = 2$. Because of the strong coupling, the $S^T = 2$ state remains unoccupied while about 30% of the molecules are in the $S^T = 1$ state at room temperature. The experimental data of magnetic measurements were confirmed by quantum chemical calculations, which both point to an antiferromagnetic coupling within the V(III) dimer.

Conflicts of interest

The authors declare no conflict of interest.

Acknowledgements

References

1 J. A. Chipman and J. F. Berry, *Chem. Rev.*, 2020, **120**, 2409–2447.

2 (*a*) S. G. Green, C. Jones and A. Stasch, *Science*, 2007, **318**, 1754–1757; (*b*) M. Bochmann, G. Wilkinson, A. M. R. Galas, M. B. Hursthouse and K. M. A. Malik, *J. Chem. Soc., Dalton Trans.*, 1980, 1797–1799; (*c*) M. L. Green, J. D. Hubert and P. Mountford, *J. Chem. Soc., Dalton Trans.*, 1990, 3793–3800; (*d*) J. N. Van Niekerk and F. R. L. Schoening, *Nature*, 1953, **171**, 36–37.

3 F. A. Cotton, E. A. Hillard and C. A. Murillo, *J. Am. Chem. Soc.*, 2003, **125**, 2026–2027.

4 (*a*) F. A. Cotton and D. J. Timmons, *Polyhedron*, 1998, **17**, 179–184; (*b*) F. A. Cotton, L. M. Daniels and C. A. Murillo, *Inorg. Chem.*, 1993, **32**, 2881–2885; (*c*) F. A. Cotton and M. Millar, *J. Am. Chem. Soc.*, 1977, **99**, 7886–7891.

5 (*a*) S. Gambarotta, M. Mazzanti, C. Floriani and M. Zehnder, *J. Chem. Soc., Chem. Commun.*, 1984, 1116–1118; (*b*) D. Fenske, A. Grissinger, M. Loos and J. Magull, *Z. Anorg. Allg. Chem.*, 1991, **598**, 121–128; (*c*) C. M. Bolinger, J. Darkwa, G. Gammle, S. D. Gammon, J. W. Lyding, T. B. Rauchfuss and S. R. Wilson, *Organometallics*, 1986, **5**, 2386–2388; (*d*) I. L. Eremenko, A. S. Katugin, A. A. Pasynskii, Y. T. Struchkov and V. E. Shklover, *J. Organomet. Chem.*, 1988, **345**, 79–86.

6 (*a*) I. L. Eremenko, A. A. Pasynskii, A. S. Katugin, O. G. Éllert, V. E. Shklover and Y. T. Struchkov, *Bull. Acad. Sci. USSR, Div. Chem. Sci.*, 1984, **33**, 1531–1532; (*b*) T. R. Halbert, L. L. Hutchings, R. Rhodes and

E. I. Stiefel, *J. Am. Chem. Soc.*, 1986, **108**, 6437–6438; (*c*) S. C. Sendlinger, J. R. Nicholson, E. B. Lobkovsky, J. C. Huffman, D. Rehder and G. Christou, *Inorg. Chem.*, 1993, **32**, 204–210.

7 C. Schöttle, P. Bockstaller, R. Popescu, D. Gerthsen and C. Feldmann, *Angew. Chem., Int. Ed.*, 2015, **54**, 9866–9870.

8 (*a*) S. Riegsinger, R. Popescu, D. Gerthsen and C. Feldmann, *Chem. Commun.*, 2022, **58**, 7499–7502; (*b*) D. Bartenbach, O. Wenzel, R. Popescu, L.-P. Faden, A. Reiß, M. Kaiser, A. Zimina, J.-D. Grunwaldt, D. Gerthsen and C. Feldmann, *Angew. Chem., Int. Ed.*, 2021, **60**, 17373–17377; (*c*) A. Egeberg, L.-P. Faden, A. Zimina, J.-D. Grunwaldt, D. Gerthsen and C. Feldmann, *Chem. Commun.*, 2021, **57**, 3648–3651; (*d*) A. Egeberg, T. Block, O. Janka, O. Wenzel, D. Gerthsen, R. Pöttgen and C. Feldmann, *Small*, 2019, **15**, 1902321.

9 (*a*) C.-C. Yang, W.-L. Huang, Y.-H. Lin, C.-Y. Wenig, Z.-Y. Mo and Y.-Y. Chen, *IEEE Trans. Magn.*, 2011, **47**, 3535–3537; (*b*) A. B. Phillips, G. Myeni and B. S. Shivaram, *AIP Conf. Proc.*, 2006, **837**, 250–254.

10 R. Zacharia, K. Y. Kim, A. K. M. Fazle Kibria and K. S. Nahm, *Chem. Phys. Lett.*, 2005, **412**, 369–375.

11 (*a*) C. Janiak, *Z. Naturforsch., B: Chem. Sci.*, 2013, **68**, 1059–1089; (*b*) E. Redel, R. Thomann and C. Janiak, *Chem. Commun.*, 2008, 1789–1791.

12 (*a*) E. Ahmed and M. Ruck, *Coord. Chem. Rev.*, 2011, **255**, 2892–2903; (*b*) M. C. Buzzeo, R. G. Evans and R. G. Compton, *ChemPhysChem*, 2004, **5**, 1106–1120.

13 H. E. Swanson, H. F. McMurdie, M. C. Morris, E. H. Evans, B. Paretzkin, J. H. DeGroot and S. J. Carmel, *Natl. Bur. Stand. (U.S.) Monogr.*, 1971, **9**, 58.

14 (*a*) G. Frenzen, W. Massa, T. Ernst and K. Dehnicke, *Z. Naturforsch., B: Chem. Sci.*, 1990, **45**, 1393–1397; (*b*) M. Plate, G. Frenzen and K. Dehnicke, *Z. Naturforsch., B: Chem. Sci.*, 1993, **48**, 149–155; (*c*) U. Kynast, S. G. Bott and J. L. Atwood, *J. Coord. Chem.*, 1988, **17**, 53–61.

15 (*a*) C. D. Beard, L. Carr, M. F. Davis, J. Evans, W. Levason, L. D. Norman, G. Reid and M. Webster, *Eur. J. Inorg. Chem.*, 2006, 4399–4406; (*b*) M. C. Durrant, S. C. Davies, D. L. Hughes, C. Le Floc'h, R. L. Richards, H. R. Sanders, N. R. Champness, S. J. Pope and G. Reid, *Inorg. Chim. Acta*, 1996, **251**, 13–14.

16 A. Ross, D. C. Soares, D. Covelli, C. Pannecouque, L. Budd, A. Collins, N. Robertson, S. Parsons, E. De Clercq, P. Kennepohl and P. J. Sadler, *Inorg. Chem.*, 2010, **49**, 1122–1132.

17 I. S. Lee and J. R. Long, *Dalton Trans.*, 2004, 3434–3436.

18 H. Lueken, in *Magnetochemie*, ed. B. G. Teubner, Stuttgart, Leipzig, 1999, p. 319.

19 A. Abragam and B. Bleaney, *Electron Paramagnetic Resonance of Transition Ions*, Clarendon Press, Oxford, 1970.

20 (*a*) K. Kanamori, *Coord. Chem. Rev.*, 2003, **237**, 147–161; (*b*) J. R. Rambo, S. L. Castro, K. Folting, S. L. Bartley, R. t A. Heintz and G. Christou, *Inorg. Chem.*, 1996, **35**, 6844–6852.

21 N. N. Nair, E. Schreiner, R. Pollet, V. Staemmler and D. Marx, *J. Chem. Theory Comput.*, 2008, **4**, 1174–1188.

22 Y. Kitagawa, T. Saito, Y. Nakanishi, Y. Kataoka, T. Matsui, T. Kawakami, M. Okumura and K. Yamaguchi, *J. Phys. Chem. A*, 2009, **113**, 15041–15046.

23 P. Hou, S. Peschtrich, N. Huber, W. Feuerstein, A. Bihlmeier, I. Krummenacher, R. Schoch, W. Klopper, F. Breher and J. Paradies, *Chem. Europ. J.*, 2022, **28**, e202200478.

24 K. Fink and V. Staemmler, *Mol. Phys.*, 2013, **111**, 2594–2605.

25 T. Bodenstein, A. Heimermann, K. Fink and C. van Wüllen, *ChemPhysChem*, 2022, **23**, e202100648.

26 N. F. Chilton, R. P. Anderson, L. D. Turner, A. Soncini and K. S. Murray, *J. Comput. Chem.*, 2013, **34**, 1164–1175.